Journal of Materials Chemistry A

Accepted Manuscript

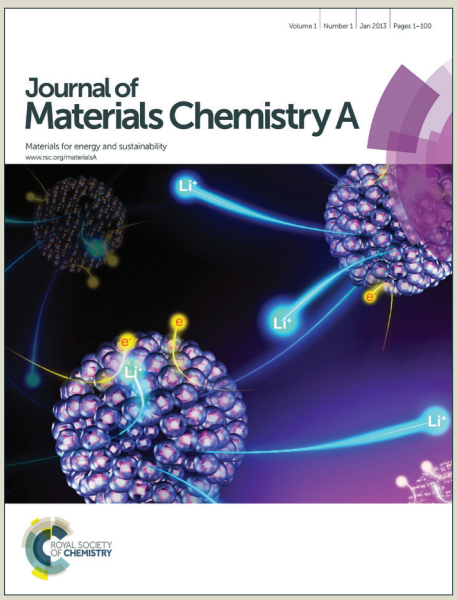

ROYAL SOCIETY OF CHEMISTRY

www.rsc.org/materialsA

Journal Name

RSCPublishing

ARTICLE

Three-Dimensional Self-Branching Anatase TiO_2 Nanorods: Morphology Control, Growth Mechanism and Dye-Sensitized Solar Cells Application

Cite this: DOI: 10.1039/xoxxoooooox

Received ooth January 2012,
Accepted ooth January 2012

DOI: 10.1039/xoxxoooooox

www.rsc.org/

Weiguang Yang,[a] Yueyang Xu,[a] Ying Tang,[a] Chen Wang,[a] Yajing Hu,[a] Lu Huang,[a] Jin Liu,[a] Jun Luo,[a] Haibo Guo,[a] Yigang Chen,[a] Weimin Shi[a] and Yali Wang*[a,b]

Complex three-dimensional (3D) hierarchical nanostructures based on well-defined low-dimensional nanobranches of different sizes and exposed specific facets are highly desirable to obtain tunable physicochemical properties. Here, a facile, one-step hydrothermal method is employed to construct self-branching anatase TiO_2 (SBAT) 3D hierarchical nanostructures. By simply controlling the reaction time and weight ratio of F127/TBAH, SBAT nanorods can be obtained with a large percentage of exposed {010} facets. Based on X-ray diffraction (XRD), field emission scanning electron microscopy (FESEM) and transmission electron microcopy (TEM) analysis, a growth mechanism is proposed for the formation of such self-branching 3D nanostructures, which involves the formation of the L-shaped step-edges on the [103] surfaces and the alignment of the crystal facets (103) of anatase nanocrystals with the (103) face on the tips of the main anatase TiO_2 nanorods. The dye-sensitized solar cell assembled with the SBAT nanorods exhibits an outstanding power conversion efficiency of 7.17%, which is superior to that of the devices based on the 1D anatase TiO_2 nanorods and P25 TiO_2. The high performance can be attributed to the high dye-uptake density, large size and unique self-branching 3D hierarchical nanostructures built from 1D nanobranches growing epitaxially from the main rod.

Introduction

Recently, titanium dioxide (TiO_2) with tailor-made crystal facets and morphology has attracted intensive interest because its photoelectric and photocatalytic properties can be further enhanced or optimized by tailoring the surface atomic structures, phase composition, crystallite size, organization and surface area.[1-14] For instance, Lu and co-workers synthesized anatase TiO_2 single crystals with mainly exposed {001} facets and demonstrated that the {001} facets are much more reactive than {101} facets for the production of H_2 from water splitting.[15,16] The works on photoanodes of dye-sensitized solar cells (DSSCs) found out that the anatase {001} facets can increase the dye-uptake due to the higher density of 5-fold-coordinnated Ti atoms on the (001) facets.[17,18] Wu et al. reported rhombic-shaped anatase TiO_2 with 43.4% {010} facets and exhibited conspicuous photocatalystic activity.[19] Moreover, Wen et al. obtained anatase TiO_2 nanocrystals exposed {010} facets via hydrothermal treatment of titanate nanosheets and discovered that the {010} facets show high photocatalytic activity and high ruthenium dye adsorption ability.[20] Recently, tetragonal faceted anatase nanorods with exposed {010} facets prepared from Na-titanate precursor exhibited enhanced photocatalytic activity.[21] Although the surface energy of {001} (0.90 J m^{-2}) is much higher than that of {010} (0.53 J m^{-2}) and {101} (0.44 J m^{-2}), theoretical and experimental studies demonstrated that {010} facets have the highest catalytic activity among {001}, {010} and {101} facets.[17,18,22-25] Therefore, it is highly desirable to achieve the aspect ratio-controlled synthesis of well-faceted anatase TiO_2 rods mainly enclosed by {010}. Nevertheless, owing to the instability of {010} with high surface energy during the crystal growth, it remains a challenge to prepare tetragonal faceted anatase rods with dominantly exposed {010} facets. Yet, most

synthesis methods of {010}-rich well-defined anatase rods require tedious two-step reactions.[14,20,21]

In addition, it is noteworthy that a substantial amount of research work has recently been devoted to controlled synthesis of three-dimensional (3D) hierarchical structures built from one-dimensional (1D) nanoscale building blocking.[26-39] Nanorods-based 3D hierarchically-structured TiO_2 can be prepared through the following approaches: vapor depostion,[31,32] vapor oxidation,[33] two-step solution,[34-37] and one-step hydrothermal.[38,39] In these cases, one-step hydrothermal is the most simple method and most of the as-prepared products are rutile TiO_2, which is the most thermodynamically stable among the three polymorphs: anatase, rutile and brookite. However, rutile usually shows inferior photovoltaic performance compared to anatase TiO_2 due to the lesser amount of adsorbed dye and slower electron transport rate.[40-42] Moreover, producing nanorods-based 3D hierarchically-structured TiO_2 is highly desirable to increase the surface areas for enhanced dye adsorption. Nonetheless, in this work, we report a facile one-step hydrothermal approach to produce self-branching anatase TiO_2 (SBAT) 3D hierarchical nanostructures with large percentage of exposed {010} facets, which shows a lower surface area compared to non-branched 1D anatase TiO_2. Analogous hyperbranched hierarchical nanostructures have recently been reported for asymmetric crystal structures (e.g., TiO_2,[43] Bi_2S_3,[44,45] Co_2P,[46] Fe_2P,[47] $BaWO_4$,[48] $LnVO_4$ (Ln = Ce, Nd)[49] and β-FeO(OH)[50]) by several research groups. They attributed the formation of such hierarchical nanostructures to crystal splitting, which is regarded as one of the main origins for formation of fractal crystals and self-assembly hierarchical nanostructures. However, one important growth mechanism to induce crystal branching can employ oriented attachment.[38,39,51,52] As is known, it is a challenge to distinguish between shape evolution during crystal growth and the oriented growth mechanism.[45] We propose a growth mechanism of the self-branching 3D nanostructures based on crystallographic alignment of the 1D nanobranches surfaces with the main rod crystal facets. The as-obtained SBAT exhibits promising behavior in DSSCs, giving rise to an outstanding power conversion efficiency of 7.17%, superior to that of the DSSCs based on the 1D anatase TiO_2 nanorods and P25 TiO_2. It can be ascribed to the high dye-uptake density, large size and unique self-branching 3D hierarchical nanostructures built from 1D nanobranches growing epitaxially from the main rod.

Experimental Section

Materials

All chemicals were used as received without any further purification. Poly(ethylene oxide)$_{100}$-poly(propylene oxide)$_{65}$-poly(ethylene oxide)$_{100}$ (F127) was obtained from Fluka, other reagents were of analytical purity and were from Sigma Aldrich.

Synthesis of Materials

In a typical synthesis, 1.8 g of F127 was first dissolved in 20 g of tetrabutylammonium hydroxide solution (TBAH, 10 wt%) with ultrasonic stirring. The weight ratio of F127/TBAH was 0.9 in all case. After a transparent solution was obtained, 4 mL of tetrabutyltitanate (TBOT) was added into the above solution and then magnetically stirred for 30 min at room temperature. The mixed solution was transferred to a Teflon-lined stainless steel autoclave and heated at 180 ^oC for different reaction times, *i.e.*, 1, 6, 8, 12, and 24 h. After reaction, the products were obtained by centrifugation, followed by rinsing with ethanol and deionized water for several times. Finally, the products were dried at 70 ^oC for further use.

Fabrication of Photoanodes

The as-produced TiO_2 paste was obtained by adding 0.5 g of the as-produced TiO_2 into 0.8 g of 5 wt% hydroxypropyl cellulose of diethylene glycol solution and stirred for 2 days at 60 ^oC. The resulting paste was spread onto the FTO glass by doctor blading using Scotch tape as frame and spacer to control film thickness, dried at 200 ^oC for 10 min and subsequently heated in air for 40 min at 490 ^oC. After cooled to 80 ^oC, the as-produced TiO_2 film was sensitized with a dry ethanol containing 0.3 mM N719 over night.

Solar cell Fabrication

To make a reasonable comparison, the thickness and active area of all the anode films were about 13 μm and 0.20 cm^2, respectively. To assemble the solar cells, a Pt-coated conducting glass was placed on the sensitized TiO_2 film separated by a 50 μm thin membrane spacer. The assembled cell was then clipped together as an open cell. An electrolyte, which was made with 0.1 M LiI, 0.05 M I_2, 0.6 M dimethylpropylimidazolium iodide (DMPImI) and 0.5 M tert-butylpyridine in a dry mixed solution (acetonitrile : valeronitile = 85 : 15) was injected into the open cell from the edges by capillarity.

Characterization

The as-prepared TiO_2 were characterized with use of field emission scanning electron microscope (FESEM, JEOL, JSM-6700F), high-resolution TEM (HRTEM, JEOL, JEM-2010F operated at 200 kV), X-ray powder diffraction (XRD, Rigaku D/max-2200V diffractometer with CuKαradiation, λ=0.1541, 40 kV, 40 mA), UV-vis spectrophotometer (Lamda-2), and BET (Micrometrics ASAP 2020). Photocurrent-voltage measurements were performed under an illumination of 100 mW cm^{-2} with simulated AM 1.5 solar simulator (Newport Oriel Solar Simulator).

Results and discussion

Preparation and Characterizations of SBAT Nanorods

SBAT nanostructures can be synthesized by a facile, one-step hydrothermal method. SEM and TEM images of corresponding branched nanostructures (Fig. 1) show the morphological features of SBAT synthesized with a reaction time of 24 h. The length of the self-branching TiO_2 nanorods was 0.7-2.3 μm with a core nanorod and dense primary nanobranches growing from both ends of the core rod with different radial angles. Further observation reveals that the nanobranches atop were parallel to the long axis of the main rod which is evident from the HRTEM observation, whereas the nanobranches surrounding the side surface of the main rod tended to be tilted with the long axis of the main rod. HRTEM image (Fig. 1d) of the area marked by a dashed red square in panel c shows there were four primary nanorods. The phase and crystal structure of the primary nanorods were confirmed by the lattice image of Fig. 1d. The distance between lattice fringes was assigned to

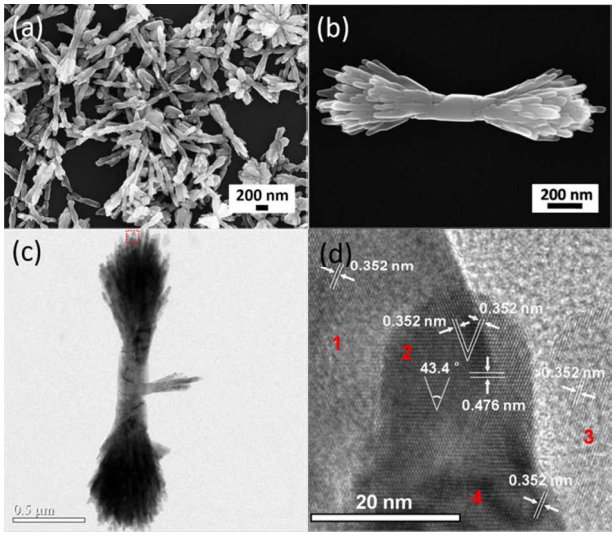

Fig. 1(a) SEM image of SBAT synthesized for 24 h. (b) SEM and (c) TEM images of individual SBAT nanorod. (d) HRTEM image obtained from the region which is marked using the red dashed square in panel c.

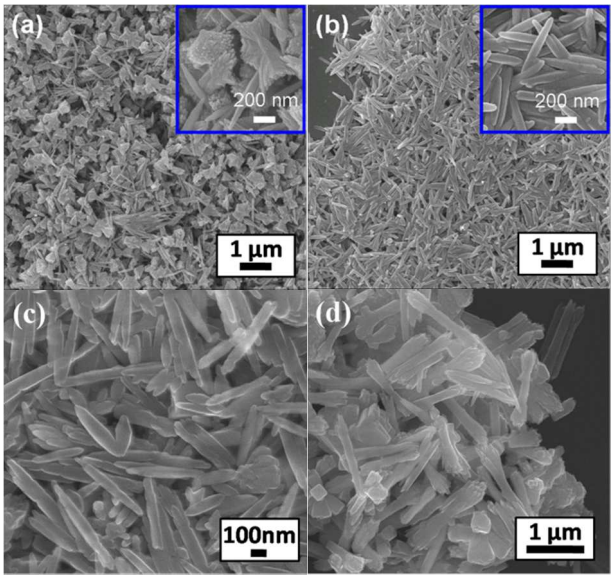

Fig. 3 SEM images of the four samples prepared for (a) 1 h, (b) 6 h, (c) 8 h, and (d) 12 h. The insets show their high-magnification SEM pictures.

(101) and (001) of the anatase TiO_2 phase. The crystalline distances were exactly consistent with d_{101} = 0.352 nm and d_{001} = 0.476 nm of the anatase TiO_2 phase. The interfacial angle of 43.4° were agreement with the angle of (101) and (-101) planes. The primary nanorods were of perfect single-crystal nature, which grew along the *c* axis and exposed with (010) plane. The (101) planes of the four primary nanorods were almost parallel to each other. It might suggest that the primary nanorods grew epitaxially from the core rod, reflecting a certain interfacial crystallographic relationship between the core rod and nanobranches.

The as-synthesized samples were examined with X-ray diffraction (XRD), and their patterns (Fig.2) show all the XRD peaks matched well with the crystal structure of the anatase TiO_2 phase (space group $I4_1/amd$, JCPDS card no. 21-1272)[53] and no other phases can be detected. The XRD intensity of the sample prepared for 1 h was much lower than that of the other sample with different reaction time from 6 h to 24 h, which is closely related with their shapes and crystallinities. The (004) and (200) peaks were respectively used to estimate the lengths of the crystal-stacking domain along *c* and *a*-axes of the anisotropic particles (Fig. 2b). The intensity ratios of (004)/(200) was shifted from 1.00 for the sample obtained in 1 h to 0.86, 0.65, 0.71 and 0.75 for the samples prepared for 6, 8, 12 and 24 h, respectively. Such features hint that the as-prepared samples had a preferred growth orientation along the *c*-axes of the

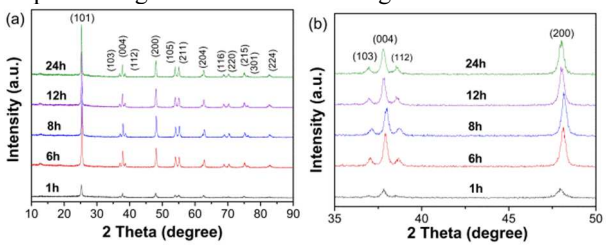

Fig. 2 (a) XRD patterns of as-prepared samples with different reaction time from 1h to 24 h. (b) Magnified view of XRD patterns between 2θ values of 35 and 45°.

anatase lattice and their anisotropic growth changed with increasing reaction time.

A series of hydrothermal experiments with different reaction time were carried out to investigate the time-dependent morphological evolution of the as-obtained anatase TiO_2. We found that the formation of self-branching nanostructures was strongly dependent on the reaction time. As shown in Fig.3a, when the reaction duration was as short as 1 h, 600-nm-sized starfish-like anatase TiO_2 nanospindle aggregates coexisted with anatase TiO_2 nanospindles (Nanospindle-based TiO_2 (NSBT) is named to refer to the sample prepared for 1 h) with a uniform diameter of about 70 nm and length of about 700 nm. When the reaction was prolonged to 6 h (Fig. 3b), the starfish-like nanospindles-based aggregates disappeared and the sample was composed entirely of well-faceted anatase TiO_2 nanorods (ATN) with a main diameter of about 80 nm and length of about 600 nm. On further increasing reaction time from 6 h to 8 h (Fig. 3c), a mixture of non-branched nanorods which exhibited a wide size distribution with a main diameter of about 50 nm and length of about 490 nm and 70-125 × 500-810 nm-sized branched TiO_2 nanorods composed of few primary nanorods was obtained. One can observe that the non-branched nanorods had a smaller size than the nanorods obtained in 6 h while the size of the branched TiO_2 nanorods increased with an increase in the amount of their primary nanobranches. After the reaction evolved for 12 h (Fig. 3d), the as-obtained sample almost exclusively contained branched TiO_2 nanorods with the length of 0.7-1.5 μm whose primary branches were denser than the sample prepared for 8 h but less dense than the sample prepared for 24 h. The more detailed structural information of the as-prepared products synthesized with different reaction time were further analyzed by TEM and selected-area electron diffraction (SAED) measurements.

Fig. 4a shows a typical TEM image at low magnification of anatase particles prepared for 1 h, revealing that the anatase particles were composed of nanospindles-based aggregates and spindles, consistent with SEM observations. A high-resolution TEM (HRTEM) image of a single spindle shows the lattice fringes with the spacing of 0.352 and 0.476 nm were respectively ascribed to (101) and (002) planes of anatase TiO_2,

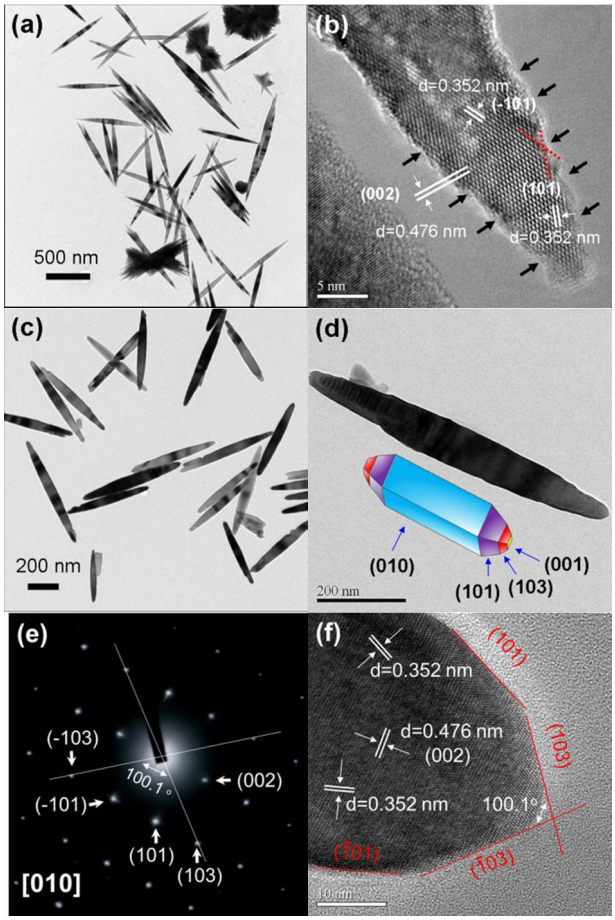

Fig.4 Representative TEM images of the samples prepared for 1 h and 6 h. (a and c) low-magnification TEM image of the samples prepared for 1 h and 6 h. (b) high-resolution TEM image of single spindle prepared for 1 h. (d) low-magnification TEM image, (e) corresponding SAED pattern and (f) high-resolution TEM image recorded from single nanorod prepared for 6 h. Inset of (d): Schematic illustration of the anatase crystal planes of the nanorod.

indicating the preferred growth along the *c* axis (Fig. 4b).[19] The surface profile image of the spindle showed stepped terraces on the [101] surface, which were marked with black arrows. The stepped surface of the spindle was facetted with TiO_2 anatase {101} faces as shown by red lines. Such saw-tooth shape of the spindle with the inclined {101} surface indicated that the spindle-like structure was formed through oriented attachment occurring in the <001> direction.[54] With the extension of reaction time up to 6 h, only anatase TiO_2 nanorods with 40 to 80 nm in lateral size and 340 to 740 nm in longitudinal size were left (Fig. 4c), which well agrees with SEM results. Fig. 4d shows a TEM image of a representative single rod with a size of about 90 × 740 nm. The corresponding selected-area electron diffraction (SAED) pattern (Fig. 4e) can be indexed by the diffraction from the [010] zone axis, indicating the single-crystal nature of the rod and preferred growth direction along the *c* axis.[19,21,55] Fig. 4f shows an HRTEM image of the rod tip, further confirming its single-crystal nature. The tip was truncated cone-like, and it was terminated by five different lattice planes. The three sets of lattice fringes with spacing of 0.352, 0.476 and 0.352 nm can be assigned to (101), (002) and (-101) planes of anatase TiO_2. An angle of 100.1° observed on the rod tip was consistent with the theoretical value for the interfacial angle between (103) and (-103) facets, indicating

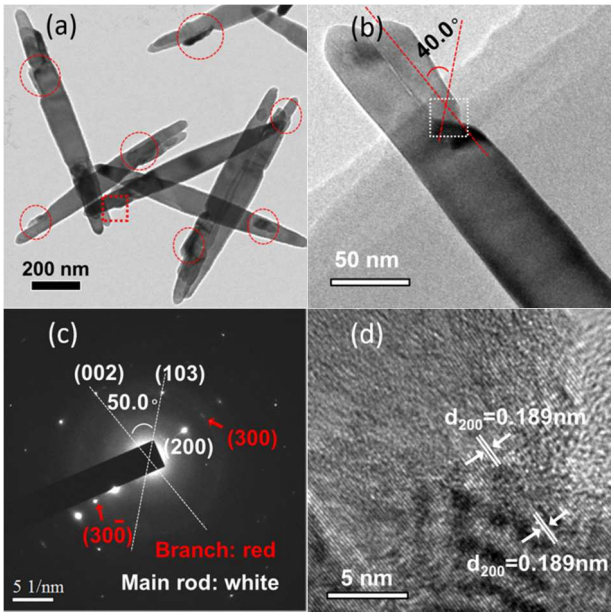

Fig. 5(a) TEM image of the nanorods prepared for 8 h. TEM image (b) and its corresponding SAED (c) of an individual branched nanorod. (d) HRTEM image of branch-main rod interface marked by the white doted square in Fig. 5b.

that the rod exhibited flat facets of {103}. The result can be confirmed by SAED observation. Based on the SEM, TEM and SAED results together with the crystallographic symmetries of anatase, we can conclude that the anatase TiO_2 nanorods were enclosed by lateral {010}, {101}, {103} and top {001} facets (see the inset in Fig. 4d).

As mentioned above, one significant feature observation in Fig. 1 is that the growth directions of nanobranches atop the main rod seem to be parallel to the c-axis of the main rod, suggesting a certain defined relationship between the crystalline main rod and nanobranches. To further understand the relationship between the morphological transformation of TiO_2 particles and such structural relationship, we applied TEM to carefully examine the branched structure and particularly the connecting interfaces of the sample prepared for 8 h. Fig. 5a shows a typical overview image of anatase TiO_2 rods with few small nanobranches marked by the red dashed circles, demonstrating the earlier stage of the formation process of branched nanostructures. In this growth stage, an L-shaped step-edge at the tip of the anatase TiO_2 rods was formed as indicated by a red dotted square in Fig. 5a, and small nanobranches marked by the red dashed circles started to grow from the corner of L-shaped step-edges. Closer observation (Fig. 5b) found that the long axis of nanobranch was parallel to that of the main rod and exhibited a 40° angle with respect to the normal of the nanobranch/main rod boundary. The SAED patterns (Fig. 5c) recorded from the nanobranch/main rod junction shows that the (200) planes of the main rod were parallel to the (300) planes of the nanobranch and the interfacial angle of (002) and (103) planes was 50° which is equal to that of the long axis of nanobranch and the interface between the nanobranch and main rod, indicating the nanobranch epitaxially grew from the main rod and its (103) crystal facet was aligned with (103) facet of the main rod. An HRTEM image recorded from the nanobranch/main rod junction further confirms the perfect epitaxial growth (Fig. 5d).

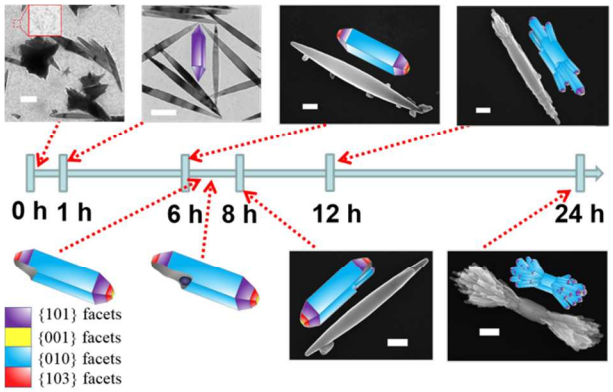

Fig. 6 Schematic representation of the formation and shape evolution of SBAT nanorods. Scale bars: 200 nm.

Growth Mechanism of SBAT

Based on the experimental observations, we propose a possible formation mechanism of self-branching anatase TiO_2 nanorods, as shown in Fig. 6. The final morphology of TiO_2 crystals is related to both their crystal growth habit and reaction condition, such as reaction solvents, reaction time, surfactants and so on.[56-59] It is generally believed that the growth habit of TiO_2 crystals under solution condition highly depends on the relative order of surface energies.[15-19] For anatase TiO_2 crystals, the surface energy decreases in the order of $\gamma\{001\}$ (0.90 J/m^2) > $\gamma\{103\}$ (0.83 J/m^2) > $\gamma\{010\}$ (0.53 J/m^2) > $\gamma\{101\}$ (0.44 J/m^2).[60,61] As the primary driving force for crystal growth, reduction in surface energy leads to anisotropic growth due to different surface energies of various crystal planes.[62] Further reduction in surface energy leads to crystal morphology evolution due to minimization of the area of high surface energy faces.[63] In the present work, the morphology evolution of anatase TiO_2 particles strongly depends on the reaction duration, keeping other parameters including reaction temperature, concentrations of precursor, and weight ratio of F127/TBAH fixed. After 10 min of reaction at 180 °C, the reaction solution started to become turbid and a large amount of tiny nanoparticles coexisted with a small amount of starfish-like anatase TiO_2 nanopindles aggregates and anatase TiO_2 nanospindles (top-left side in Fig. 6). The formation of spindle-like nanostructures seems to be driven by the minimization of the overall surface energies via orientation attachment,[55,64] which is regarded to generally exist in the early stage of crystal growth, leading to the fusion of several particles into a single crystal by sharing a common crystallographic orientation, despite the present of strong surface-bound ligands.[65,66] In our previous work, we found that high concentration of TBAH can induce anisotropic growth of TiO_2 particles via orientation attachment, leading to the formation of anatase rod-shaped TiO_2.[55] After the reaction for 1 h at this temperature, the starfish-like anatase TiO_2 nanopindles aggregates coexisting with anatase TiO_2 nanospindles became dominant and the anatase TiO_2 nanospindles were dominantly enclosed by stepped terraces on the [101] surface, leading to nearly 100% percentage of exposed {101} facets. With an increase in reaction time to 6 h, the starfish-like anatase TiO_2 nanopindles aggregates coexisting with anatase TiO_2 nanospindles completely transformed into anatase TiO_2 tetragonal faceted-nanorods enclosed by lateral {010}, {101}, {103} and top {001} facets. In our reaction system, Bu_4N^+ cations generated from TBAH can selectively adhere to particular crystal facets such as {010}, {103} facets, and hinder their growth.[55] Meanwhile, OH^- anions coming from TBAH preferentially adsorbed onto {010} facets forming O-terminated {010} facets and thereby thermodynamically stabilized the {010} facets, resulting in the large percentage of exposed {010} facets.[60,67,68] As a cosurfactant, block copolymer F127 can wholly cap the surface of TiO_2 particles. It was reported that F127 plays a vital role in anisotropic self-assembly of TiO_2 nanoparticles via orientation attachment proceeding on the {200} planes.[69] However, we found that in a controlled experiment, with an increase in the weight ratio of F127/TBAH from 0.9 to 1.0, no self-branching nanostructures were observed after 24 h of reaction time (Fig. S1a, ESI†). Further increasing the weight ratio of F127/TBAH to 1.1 with 24 h of reaction time led to a mixture of nanorods and particles of irregular shape, which was composed of anatase (97.3%) and rutile (2.7%) (Fig. S1b, ESI†). When the weight ratio of F127/TBAH reached 1.4, particles of irregular shape consisting of 47.8% anatase and 52.2% rutile can exclusively be obtained in 24 h of reaction time (Fig. S1c, ESI†). Therefore, a sufficient quantity of F127 might tightly and wholly bind to the surface of TiO_2 particles and hinder the selective absorption of organic amines and OH^- anions from TBAH onto the specific facets of TiO_2 particles, leading to the failure of the anisotropic growth. With a further increase in reaction time (more than 6 h) under 0.9 of the weight ratio of F127/TBAH, L-shaped step-edges are found to be formed (bottom-left side in Fig. 6). This might be due to that it took a considerably long time (more than 6 h) for F127 below its critical concentration to break the equilibrium adsorption on the surfaces of anatase TiO_2 nanorods, resulting in the exposure of the surfaces without F127 capping on the tips of anatase TiO_2 nanorods and then OH^- anions from TBAH can selectively etch the exposed clean surfaces, forming the L-shaped step-edges on the [103] surfaces. To further reduce the surface energy of the reaction system, the crystal facets (103) of anatase TiO_2 nanoparticles preferred to be aligned with the (103) face of the L-shaped step-edges of the anatase TiO_2 nanorods, forming nanobranches growing along the direction parallel to the long axis of the main anatase TiO_2 nanorods. Such preferential growth explains the formation of nanobranches parallel to the c-axis of the main rod. However, it does not seem to explain the formation of nanobranches with tilted angles to the c-axis of the main rod. We think crystal splitting is most likely responsible for the formation of the nanobranches. In general, crystal splitting is associate with both thermodynamic and kinetic factors: variation in the total free energy of crystal growth, extra molecules appearing in the reaction system and fast crystal growth depending strongly on the reaction solution oversaturation.[43-50] The extra amount of surfactants and occurrence of crystal etching might produce a large amount of surfactant-passivated monomers, leading to fast crystal growth. The violent growth fluctuations within the solution layer most close to the starting seeds would locally accelerate monomers addition to the {103} surface with the highest energy among the exposed surfaces, leading to the nanocrystal splitting to form the nanobranches.[43] Conflicting with the previous results,[43,45-49] we increased the amount of F127 surfactant, leading to the failure of the formation of crystal splitting. It may be due to that the increase in F127 amount prohibits the crystal etching and changes the thermodynamic stability order of the possible TiO_2 polymorphs which is confirmed by the XRD results (Fig. S1, ESI†). In addition, the dislocations at interfacial connection

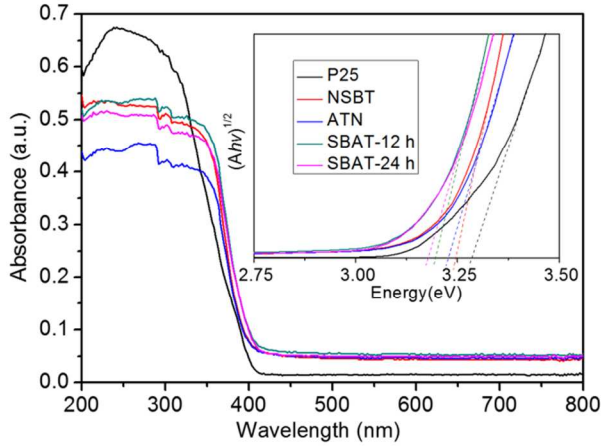

Fig.7 Optical UV-visible adsorption spectra of NSBT, ATN, SBAT prepared for 12h (SBAT-12h), SBAT prepared for 24h (SBAT-24h) and commercial P25 and the inset is their corresponding plots of transformed Kubelka-Munk function vs. the energy of light.

confirmed by the TEM observation of Fig. S2 (ESI†) tend to induce crystal splitting, leading to the formation of nanobranches.[70]

Optical Properties

Fig. 7 shows the UV-visible spectra of NSBT, ATN, SBAT-12 h, SBAT-24 h and commercial P25 TiO_2. The band gap energies are as follows: for P25 TiO_2, the band gap is 3.28 eV, for NSBT it is 3.25 eV, for ATN it is 3.23eV, for SBAT-12 h it is 3.20 eV, and for SBAT-24 h it is 3.18eV. It indicates that the intrinsic absorption edge of the as-prepared samples with different reaction times (1-24 h) had an obvious red-shift compared to P25 TiO_2 and a sequential red shift of absorption band edge from 3.25 to 3.18 eV occurs with increasing the reaction time.

Cell Performances

Fig. 8 shows the photocurrent density-voltage (*J-V*) characteristics of the DSSCs based on NSBT, ATN, SBAT-12 h, SBAT-24 h and P25 TiO_2 under simulated illumination (100 mW/cm^2, AM 1.5G). The surface area, dye-uptake densityand

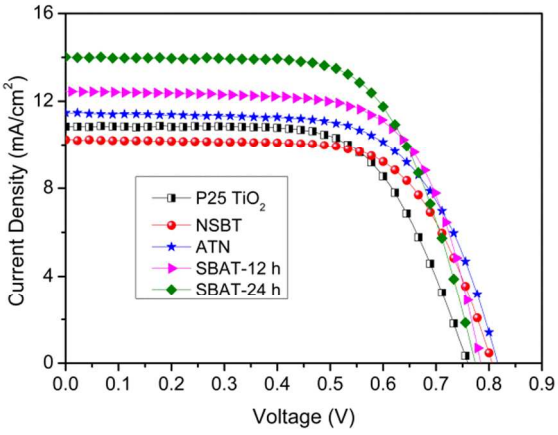

Fig. 8 Photocurrent-voltage curves measured using NSBT, ATN, SBAT prepared for 12 h (SBAT-12 h), SBAT prepared for 24 h (SBAT-24 h) and P25 TiO_2 as photoanodes.

Table 1 Surface area, dye-uptake density and cell parameters of the dye-sensitized solar cells (DSSCs) based on NSBT, ATN, SBAT-12 h, SBAT-24 h and P25 TiO_2[a]

sample	BET (m^2/g)	dye uptake density[b] (×10-7 mol/m^2)	Voc (V)	Jsc (mA/cm^2)	FF	η (%)
P25 TiO_2	50.3	1.71	0.76	10.84	0.65	5.36
NSBT	23.1	1.22	0.80	10.24	0.67	5.52
ATN	17.1	4.36	0.81	11.48	0.65	6.08
SBAT-12h	11.4	5.12	0.78	12.45	0.69	6.66
SBAT-24h	11.1	5.49	0.77	14.01	0.67	7.17

[a]The V_{oc}, J_{sc}, FF, and $\eta$are open circuit voltage, short circuit current density, fill factor, and power conversion efficiency of the DSSCs, respectively. The active areas of the photoanodes are about 0.20 cm^2 for all the tested cells; [b]Dye uptake density is the dye uptake amount per BET surface areas of the per unit weight (10 mg) samples, which is calculated by the dissolution of the dye adsorbed samples in the 10 mM NaOH solution (ethanol : water = 1:1) using UV-vis spectroscopy.

solar cell parameters including short-circuit current density (J_{sc}), open-circuit voltage (V_{oc}), fill factor (FF) and power conversion efficiency (η) are summarized in Table 1. It can be observed that the cell efficiency varied in the order SBAT-24 h > SBAT-12 h > ATN > NSBT > P25 TiO_2 as 7.17% > 6.66% > 6.08% > 5.52% > 5.36 %, respectively. It is worth noting that the J_{sc} was highest for SBAT-24 h with the lowest surface area of 11.1 m^2/g and minimum for NSBT with the second highest surface area of 23.1 m^2/g. The high surface area is desirable for great dye adsorption, which strongly affects the J_{sc}. However, in the case, the surface area may not have been a major factor in the amount of dye adsorbed. The increasing trend for J_{sc} is similar to that for dye-uptake density corresponding to dye molecules amount absorbed on the crystal surface per surface areas of the TiO_2 crystal (mol/m^2), and opposite to that for the surface areas, indicating the large percent of exposed {010} facets, large particle size and unique self-branching nanostructures play a key role in the amount of dye adsorbed, resulting in the improvement of the J_{sc}. N_2 adsorption-desorption isotherms (Fig. S3a, ESI†) showing smiliar Type II curves with a Type H4 hysteresis loop were obtained for SBAT-12 h and SBAT-24 h, demonstrating the presence of mesoporous structures. Barret-Joyner-Halenda (BJH) analyses (Fig. S3b, ESI†) show that P25 TiO_2 and self-branching TiO_2 with the reaction time of 12 and 24 h exhibited pore sizes of 85.0 and 3.5 nm, respectively. It is interesting to note that SBAT-12 h and SBAT-24 h with similar surface areas have the same pore sizes but different dye-uptake densities. This may be attributed to the variation in crystallinity caused by difference in reaction time. Compared with P25 TiO_2, the improvement in V_{oc} for SBAT-12 h and SBAT-24 h can be explained as a consequence of effective charge transport of such one-dimensional (1D) nanostructureand enhanced mass transport of the electrolyte ions in and out of the self-branching TiO_2 due to the presence of the pore size of 3.5 nm.

SBAT-24 h exhibits larger Jsc and η than that of the other samples, which can be ascribed to a couple of factors. First, there is the trade-off effect of the decreased surface areas, the enhanced light scattering due to the large particle size, and the increased dye-uptake density resulted from the large percent of exposed {010} facets having strong dye adsorption capacity[20] and large particle size possessing good adsorption behavior.[71] Second, the unique self-branching nanostructure built from 1D nanobranches growing epitaxially from the core rod can

effectively minimize the grain interface effect and thus facilitate the photogenerated electron transport.[43,72-74]

Conclusions

In summary, SBAT with a large percentage of exposed {010} facets were synthesized by a facile, one-step hydrothermal reaction using TBAH as a capping and facet-controlling agent and F127 as a capping and shape-controlling agent. The reaction time and weight ratio of F127/TBAH played an important role in controlling the structure and morphology of the as-prepared TiO_2. With increasing the reaction time from 10 min to 24 h, the formation of self-branching anatase TiO_2 nanorods involved an evolution from 0D primary nanoparticles to 1D nanorods and eventually to 3D self-branching nanostructures by means of an oriented attachment complexed with crystal splitting of anatase nanocrystals. The crystal facets (103) of anatase nanocrystals were found to be aligned with (103) face on the tips of the main anatase TiO_2 nanorods, leading to the formation of the 3D self-branching nanostructures. With increasing the weight ratio of F127/TBAH from 0.9 to 1.4, we observed the disappearance of the 3D self-branching anatase nanorods and the formation of the TiO_2 with irregular shape consisting of 47.8% anatase and 52.2% rutile.

The power conversion efficiency of the device based on the 3D SBAT could be up to 7.17%, superior to that of the devices based on the 1D anatase TiO_2 nanorods and P25 TiO_2. The improvement of the η cannot be explained by high surface area because self-branching decreased surface area. Such improvement can be arising from high dye-uptake density due to a large percentage of exposed {010} facets, high crystallinity and adequate pore size, the enhanced light scattering due to the large particle size, and the unique self-branching nanostructure built from 1D nanobranches growing epitaxially from the core rod which can effectively minimize the grain interface effect and thus facilitate the photogenerated electron transport.

Acknowledgements

The authors gratefully acknowledge the financial support of the project from the National Natural Science Foundation of China (No. 51202139), Nature Science Foundation of Shanghai (No. 12ZR1443900, No.14ZR1416400), Specialized Research Fund for the Doctoral Program of Higher education (No. 20123108120022), Special Research Foundation for Training and Selecting Outstanding Young Teachers of Universities in Shanghai (No. ZZSD12041), Innovation Foundation of Shanghai University. They also thank Mr. Pengfei Hu and Yuliang Chu (Analysis and Testing Center of Shanghai University) for their kind assistance with HRTEM and FEDEM measurements.

Notes and references

[a]Department of Electronic Information Materials, School of Materials Science and Engineering, Shanghai University, Shanghai 200444, China.
[b]Nano-Science and Nano-Technology Research Center, School of Materials Science and Engineering, Shanghai University, Shanghai 200444, China.

† Electronic Supplementary Information (ESI) available: [SEM images, XRD patterns, and TEM images for the as-prepared TiO_2]. See DOI: 10.1039/b000000x/

1 A. Testino, I. R. Bellobono, V. Buscaglia, C. Canevali, M. D'Arienzo, S. Polizzi, R.Scotti and F. Morazzoni, *J. Am. Chem. Soc.*, 2007, **129**, 3564.
2 D. Zhang, G. Li, X. Yang and J. C. Yu, *Chem. Commun.*, 2009, 4381.
3 X. Han, Q. Kuang, M. Jin, Z. Xie and L. Zheng, *J. Am. Chem. Soc.*, 2009, **131**, 3152.
4 G. Liu, L. Z. Wang, H. G. Yang, H. M. Cheng and G. Q. Lu, *J. Mater. Chem.*, 2010, **20**, 831.
5 N. Wu, J. Wang, D. N. Tafen, H. Wang, J. G. Zheng, J. P. Lewis, X. Liu, S. S. Leonard and A. Manivannan, *J. Am. Chem. Soc.*, 2010, **132**, 6679.
6 M. Liu, L. Piao, L. Zhao, S. Ju, Z. Yan, T. He, C. Zhou and W. Wang, *Chem. Commun.*, 2010, **46**, 1664.
7 T. Tachikawa, S. Yamashita and T. Majima, *J. Am. Chem. Soc.*, 2011, **133**, 7197.
8 H. B. Jiang, Q. Cuan, C. Z. Wen, J. Xing, D. Wu, X. Q. Gong, C. Li and H. G. Yang, *Angew. Chem. Int. Ed.*, 2011, **50**, 3764.
9 J. Ye, W. Liu, J. Cai, S. Chen, X. Zhao, H. Zhou and L. Qi, *J. Am. Chem. Soc.*, 2011, **133**, 933.
10 H. B. Wu, J. S. Chen, X. W. Lou and H. H. Hng, *Nanoscale*, 2011, **3**, 4082.
11 P. Wen, Z. Tao, Y. Ishikawa, H. Itoh, and Q. Feng, *Appl. Phys. Lett.*, 2010, **97,** 131906.
12 Y. Qiu, W. Chen and S. Yang, *Angew. Chem. Int. Ed.*, 2010, **49**, 3675.
13 W. Yang, J. Li, Y. Wang, F. Zhu, W. Shi, F. Wan and D. Xu, *Chem. Commun.*, 2011, **47**,1809.
14 J. Pan, X. Wu, L. Wang, G. Liu, G. Q. Lu and H. M. Cheng, *Chem. Commun.*, 2011, **47**, 8361.
15 H. G. Yang, C. H. Sun, S. Z. Qiao, J. Zou, G. Liu, S. C. Smith, H. M. Cheng and G. Q. Lu, *Nature*, 2008, **453**, 638.
16 G. Liu, C. Sun, H. G. Yang, S. C. Smith, L. Wang, G. Q.Lu and H. M. Cheng, *Chem. Commun.*, 2010, **46**, 755.
17 J. G. Yu, J. J. Fan and K. L. Lv, *Nanoscale*, 2010, **2**, 2144.
18 F.Hao, X.Wang, C.Zhou, X. J.Jiao, X.Li, J. B.Li and H. Lin, *J.Phys. Chem. C*, 2012, **116**, 19164.
19 B. Wu, C. Guo, N. Zheng, Z. Xie and G. D. Stucky, *J. Am. Chem. Soc.*, 2008, **130**, 17563.
20 P. Wen, H. Itoh, W. Tang and Q. Feng, *Langmuir*, 2007, **23**, 11782.
21 J. M. Li and D. S. Xu, *Chem. Commun.*, 2010,**46**, 2301.
22 M. Lazzeri, A. Vittadini and A. Selloni, *Phys. Rev. B*, 2002, **65**, 119901.
23 A. Beltrán, J. R. Sambrano, M. Calatayud, F. R. Sensato and J. Andrés, *Surf. Sci.*, 2001, **490**, 116.
24 M. Calatayud and C. Minot, *Surf. Sci.*, 2004, **552,** 169.
25 J. Pan, G. Liu, G. Q. Lu and H. M. Cheng, *Angew. Chem. Int. Ed.*, 2011, **50**, 2133.
26 J. Lao, J. Wen and Z. F. Ren, *Nano Lett.* 2002, **2**, 1287.
27 H. Yan, R. He, J. Johnson, M. Law, R. J. Saykally and P. Yang, *J. Am. Chem. Soc.*, 2003, **125**, 4728.
28 D. Wang, F. Qian, C. Yang, Z. Zhong and C. M. Lieber, *Nano Lett.*, 2004, **4**, 871.
29 K. A. Dick, K. Deppert, M. W. Larsson, T. Martensson, W. Seifert, L. R. Wallenberg and L. Samuelson, *Nat. Mater.*, 2004, **3**, 380.
30 H. M. Cheng, W. H. Chiu, C. H. Lee, S. Y. Tsai and W. F. Hsieh, *J.Phys. Chem. C*, 2008, **112**, 16359.

31 F. Sauvage, F. D. Fonzo, A. L. Bassi, C. S. Casari, S. Russo, G. Divitini, C. Ducati, C. E. Bottani, P. Comte and M. Gratzel, *Nano Lett.*, 2010, **10**, 2562.
32 J. Shi, Y. Hara, C. L. Sun, M. A. Anderson and X. D. Wang, *Nano Lett.*, 2011, **11**, 3413.
33 X. F. Yang, J. L. Zhuang, X. Y. Li, D. H. Chen, G. F. Ouyang, Z. Q. Mao, Y. X. Han, Z. H. He, C. L. Liang, M. M. Wu and J. C. Yu, *ACS Nano*, 2009, **3**, 1212.
34 J. K. Oh, J. K. Lee, H. S. Kim, S. B. Han and K. W. Park, *Chem. Mater.*, 2010, **22**, 1114.
35 I. S. Cho, Z. B. Chen, A. J. Forman, D. R. Kim, P. M. Rao, T. F. Jaramillo and X. L. Zheng, *Nano Lett.*, 2011, **11**, 4978.
36 W. Q. Wu, H. S. Rao, Y. F. Xu, Y. F. Wang, C. Y. Su and D. B. Kuang, *Sci. Rep.*, 2013, **3**, 1892.
37 X. Sheng, D. He, J. Yang, K. Zhu and X. Feng, *Nano Lett.*, 2014, **14**, 1848.
38 E. Hosono, S. Fujihara, H. Imai, I. Honma, I. Masaki and H. Zhou, *ACS Nano*, 2007, **1**, 273.
39 W. Q. Wu, B. X. Lei, H. S. Rao, Y. F. Xu, Y. F. Wang, C. Y. Su and D. B. Kuang, *Sci. Rep.*, 2013, **3,** 1352.
40 N. G. Park, J. van de Lagemaat and A. J. Frank, *J.Phys. Chem. B*, 2000, **104**, 8989.
41 S. Banerjee, J. Gopal, P. Muraleedharan, A. K. Tyagi and B. Raj, *Curr. Sci.*, 2006, **90**, 1378.
42 W. G. Yang, F. R. Wan, Y. L. Wang and C. H. Jiang, *Appl. Phys. Lett.*, 2009, **95**, 133121.
43 R. Buonsanti, E. Carlino, C. Giannini, D. Altammura, L. D. Marco, R. Giannuzzi, M. Manca, G. Gigliand and P. D. Cozzoli, *J. Am. Chem. Soc.*, 2011, **133**, 19216.
44 V. Stavila, K. H. Whitmire and I. Rusakova, *Chem. Mater.*, 2009, **21**, 5456.
45 J. Tang and A. P. Alivisatos, *Nano Lett.*, 2006, **6**, 2701.
46 H. Zhang, D. H. Ha, R. Hovden, L. F. Kourkoutis and R. D. Robinson, *Nano Lett.*, 2011, **11**, 188.
47 A. T. Kelly, I. Rusakova, T. Ould-Ely, C. Hofmann, A. Luttge and K. H. Whitmire, *Nano Lett.*, 2007, **7**, 2920.
48 J. He, M. Han, X. Shen and Z. Xu, *J. Cryst. Growth*, 2008, **310**, 4581.
49 H. Deng, C. Liu, S. Yang, S. Xiao, Z. K. Zhou and Q. Q. Wang, *Cryst. Growth Des.*, 2008, **8**, 4432.
50 Y. Hu and K. Chen, *J. Cryst. Growth*, 2007, **308**, 185.
51 Y. W. Jun, M. F. Casula, J. H. Sim, S. Y. Kim, J. Cheon and A. P. Alivisatos, *J. Am. Chem. Soc.*, 2003, **125**, 15981.
52 D. Zitoun, N. Pinna, N. Frolet and C. Belia, *J. Am. Chem. Soc.*, 2005, **127**, 15034.
53 H. G. Yang and H. C. Zeng, *J. Phys. Chem. B*, 2004, **108**, 3492.
54 J. Polleux, N. Pinna, M. Antonietti and M. Niederberger, *Adv. Mater.*, 2004, **16**, 436.
55 W. Yang, Y. Wang and W. Shi, *CrystEngComm*, 2012, **14,** 230.
56 Y. Q. Dai, C. M. Cobley, J. Zeng, Y. M. Sun and Y. N. Xia, *Nano Lett.*, 2009, **9**, 2455.
57 H. G. Yang, G. Liu, S. Z. Qiao, C. H. Sun, Y. G. Jin, S. C. Smith, J. Zou, H. M. Cheng and G. Q. Lu, *J. Am. Chem. Soc.*, 2009, **131**, 4078.
58 N. Roy, Y. Sohn and D. Pradhan, *ACS Nano*, 2013, **7**, 2532.
59 J. S. Chen, Y. L. Tan, C. M. Li, Y. L. Cheah, D. Luan, S. Madhavi, F. Y. Chiang Boey, L. A. Archer and X. W. Lou, *J. Am. Chem. Soc.*, 2010, **132**, 6124.
60 H. Li, A. G. Kanaras and L. Manna, *Accounts Chem. Res.*, 2013, **46**, 1387.
61 U. Diebold, *Surf. Sci. Rep.*, 2003, **48,** 53.
62 M. Lazzeri, A. Vittadini and A. Selloni, *Phys. Rev. B*, 2002, **65**, 119901.
63 D. Yuvaraj, K. Narasimha Rao and K. Barai, *Solid State Commun.*, 2009, **149**, 349.
64 R. L. Pennand J. F. Banfield, *Geochim. Cosmochim. Acta*, 1999, **63**, 1549.
65 M. Adachi, Y. Murata, J. Takao, J. Jiu, M. Sakamoto and F. Wang, *J. Am. Chem. Soc.*, 2004, **126**, 14943.
66 F. Huang, H. Zhang and J. F. Banfield, *NanoLett.*, 2003, **3**, 373.
67 J. Zhang, Y. Wang, J. Zheng, F. Huang, D. Chen, Y. Lan, G. Ren, Z. Lin and C. Wang, *J. Phys. Chem. B*, 2007, **111**, 1449.
68 G. Liu, J. C. Yu, G. Q. Lu and H. M. Cheng, *Chem. Commun.*, 2011, **47**, 6763.
69 A. S. Barnard and L. A. Curtiss, *Nano Lett.*, 2005, **5**, 1261.
70 J. Wang, S. Winardi, A. Sugawara-Narutaki, A. Kumamoto, T. Tohei, A. Shimojima and T. Okubo, *Chem. Comm.*, 2012,**48**, 11115.
71 T. P. Chou, Q. Zhang, B. Russo, G. E. Fryxell and G. Cao, *J. Phys. Chem. C,* 2007, **111**, 6296.
72 L. D. Marco, M. Manca, R. Buonsanti, R. Giannuzzi, F. Malara, P. Pareo, L. Martiradonna, N. M. Giancaspro, P. D. Cozzoli and Giuseppe, *J. Mater. Chem.*, 2011, **21**, 13371.
73 L. D. Marco, M. Manca, R. Giannuzzi, M. R. Belviso, P. D. Cozzoli and G. Gigli, *Energy Environ. Sci.*, 2013, **6**, 1791.
74 R. Agosta, R. Giannuzzi, L. D. Marco, M. Manca, M. R. Belviso, P. D. Cozzoli and G. Gigli, *J. Phys. Chem. C*, 2013, **117**, 2574.

Graphical Abstract

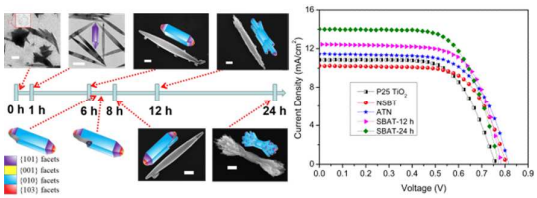

Three-dimensional self-branching anatase TiO_2 was prepared by a facile, one-step hydrothermal method for high-Performance dye-sensitized solar cells